SCIENCE CHINA
Technological Sciences

•Article•

July 2018 Vol.61 No.7: 1081–1091
https://doi.org/10.1007/s11431-017-9262-9

Flow computations of multi-stages by URANS and flux balanced mixing models

ZHU YaLu[1], LUO JiaQi[1*] & LIU Feng[1,2]

[1] *Department of Aeronautics and Astronautics, Peking University, Beijing 100871, China;*
[2] *Department of Mechanical and Aerospace Engineering, University of California, Irvine CA92697-3975, USA*

Received September 26, 2017; accepted April 23, 2018; published online June 8, 2018

The quasi-steady methods based on mixing models have been widely applied to flow computations of turbomachinery multi-stages in aerospace engineering. Meanwhile, the unsteady numerical simulation has also been used due to its ability in obtaining time-dependent flow solutions. In the paper, two different mixing treatments and the corresponding flux balanced ones are presented to exchange the flow solutions on the interfaces between adjacent blade rows. The four mixing treatments are then used for flow computations of a subsonic 1.5-stage axial turbine and a quasi-1.5-stage transonic compressor rotor. The results are compared with those by unsteady numerical method, which is implemented by using the sliding mesh technique. The effects of the quasi-steady and unsteady computation methods on the conservation of flow solutions across the interfaces are presented and addressed. Furthermore, the influence of mixing treatments on shock wave and flow separation of the transonic compressor rotor is presented in detail. All the results demonstrate that the flux balanced mixing treatments can be used for multi-stage flow computations with improved performance on interface conservation, even in the complex flows.

computational fluid dynamics, multi-stage, mixing model, flux balance, unsteady flow

Citation: Zhu Y L, Luo J Q, Liu F. Flow computations of multi-stages by URANS and flux balanced mixing models. Sci China Tech Sci, 2018, 61: 1081–1091, https://doi.org/10.1007/s11431-017-9262-9

1 Introduction

Through-flow method, mixing model, passage-averaging and unsteady computation are the typical approaches for numerical simulation of multi-stage turbomachinery flow. The through-flow method, proposed by Wu [1], decomposes the three-dimensional turbomachinery flow into a pair of two-dimensional flows, by which the flow solutions can be iteratively obtained. The mixing model method, first proposed by Denton [2], employs an interface, called mixing plane, between adjacent blade rows, where the circumferentially averaged flow solutions on each side are exchanged. This method transfers the inherent unsteady flow of multi-stages into a quasi-steady one, resulting in a balance between the significantly reduced computational cost and the fidelity of flow solutions. However, in the situations with plenty of blade rows or small axial gap between adjacent blade rows, the flow solutions by mixing models deviate from the experiments, or even no converged results can be obtained. The passage-averaging method, developed by Adamczyk [3,4], transfers the unsteady flow into the time-averaged one in a single blade passage by introducing three averaging operators in the Navier-Stokes equations. However, it is rarely applied due to the complexity and difficulty to close the correlated terms. By solving the unsteady Euler [5,6], unsteady Reynolds-averaged Navier-Stokes (URANS) equations [7–9], more flow details can be obtained. Furthermore, the turbulence flow in turbomachinery is rather complex and demonstrates a strong non-equilibrium turbulent transport nature, it is still a challenge for predicting the flow correctly

* Corresponding author (email: jiaqil@pku.edu.cn)

[10]. Hybrid LES/RANS could give more reasonable results and can be used to investigate the flow mechanism [11–14], but with enormous computational cost.

At present, the mixing model method is the most popular one in the flow computations of multi-stages. The crucial issue of mixing model method is the appropriate model used to simulate the flow mixing process on the interface between adjacent blade rows. In order to match the flow mixing process as far as possible, a practical mixing model should be able to: (1) keep strong conservation of flow solutions across the interface, such as mass flow rate, momentum, total enthalpy, etc.; (2) obtain the aerodynamic parameters with little deviation from the experiment; (3) be robust by employing non-reflective boundary conditions on the interface and special interface treatments for reversed flow. Since the 1990s, several mixing models have been introduced [15–17]. A popular class of simple mixing models simulate the flow mixing process by simply circumferentially averaging the flow variables on the interface. Since there are only five independent flow variables in three-dimensional compressible flow, different selections of the independent flow variables result in different simple mixing models.

In the past decade, some novel mixing models have also been proposed. Holmes [18] introduced a flux balance method to strongly conserve the fluxes across the interface. Wang [19] proposed an improved flux balance mixing model by introducing virtual cells on the interface. These models are used to resolve the reversed interface flow. Ning [20], Du and Ning [21] introduced a mixing model by adding a constant-radius buffer layer at each side of interface to alleviate the artificial reflection in the simple mixing models. All the results demonstrate that different mixing models have various effects on the computation robustness, flow solution conservation and thus the flow details. However, no comparative investigation of the aforementioned novel mixing models has been carried out in the open literatures.

With the development of computer capacity, more emphases are put on URANS. The unsteady computation methods for multi-stages include the phase-lagged method [5], blade scaling technique [22], time-inclined method [6] and frequency domain methods, such as nonlinear harmonic method [23] and harmonic balance method [24]. Due to the eases of implementation and extension to multi-stages, the blade scaling technique has been widely applied in the unsteady turbomachinery flow computations. The exchange of two-dimensional flow fields on the interface between adjacent blade rows is the most crucial issue for unsteady flow computation of multi-stages because of the non-matched grid points between the two sides of the interface and the relative motion between rotor and stator. In such cases, it is necessary to develop an interpolation method strongly maintaining the conservation and continuity of flow variables across the interface.

In the present study, four mixing models including two simple ones and two corresponding flux balanced ones are first implemented. An interpolation method to exchange flow solutions across the interface between adjacent blade rows is also introduced for unsteady flow computations of multi-stages. Then two test cases, a subsonic 1.5-stage axial turbine and a quasi-1.5-stage transonic compressor rotor, are investigated by using the four mixing models and URANS. The influence of the present quasi-steady and unsteady computation methods on the flow conservation across interfaces are presented in detail. The results obtained from mixing models are compared with those from URANS to evaluate the ability of flux balanced mixing models on flux conservation across interface, even in the transonic compressor flow with shock wave and flow separation.

2 Numerical methods

The three-dimensional compressible (U)RANS equations are solved in the rotating frame of reference. The Spalart-Allmaras turbulence model [25] is used to resolve the eddy viscosity. The convective and viscous fluxes are discretized by JST [26] and second-order central schemes, respectively. The Lower-Upper Symmetric-Gauss-Seidel (LU-SGS) method [27] is used for the pseudo time step. The local time-stepping and multi-grid techniques are applied to accelerate the computation. The total pressure, total temperature and flow angles at the inlet and the hub pressure at the outlet are given. The setups of interface boundary condition between adjacent blade rows for steady and unsteady computations are described in the following two subsections, respectively.

2.1 Mixing models for steady computation

In a typical mixing model, the selected five flow variables on each side of the interface are first circumferentially averaged, and then the non-reflective interface boundary conditions are determined by the averaged flow variables. Four different mixing models are introduced in the following.

(1) Momentum-averaged (MA) model. In the MA model, the axial convective fluxes across the interface are averaged

$$\begin{aligned} I_1 &= \frac{1}{A_0}\int_A \rho v_x \mathrm{d}A_x = \overline{\rho}\,\overline{v}_x, \\ I_2 &= \frac{1}{A_0}\int_A (\rho v_x v_x + p)\mathrm{d}A_x = \overline{\rho}\,\overline{v}_x\overline{v}_x + \overline{p}\,, \\ I_3 &= \frac{1}{A_0}\int_A \rho v_r v_x \mathrm{d}A_x = \overline{\rho}\,\overline{v}_r\overline{v}_x, \\ I_4 &= \frac{1}{A_0}\int_A \rho v_\theta v_x \mathrm{d}A_x = \overline{\rho}\,\overline{v}_\theta\overline{v}_x, \\ I_5 &= \frac{1}{A_0}\int_A \rho H v_x \mathrm{d}A_x = \overline{\rho}\,\overline{H}\,\overline{v}_x, \end{aligned} \tag{1}$$

where ρ, v_x, v_r, v_θ, p and H are density, velocity components

in axial, radial and tangential directions, pressure and total enthalpy, respectively; $A_0 = \int_A \mathrm{d}A_x$, and $\mathrm{d}A_x$ is the axial component of area vector on the interface. The variables with overbars stand for the corresponding averaged ones. The averaging is performed on each span to ultimately produce the spanwise distributions of averaged flow variables.

Taking into account the definition of total enthalpy, a quadratic equation in averaged pressure is obtained

$$(\gamma+1)\overline{p}^{\,2} - 2I_2\overline{p} - (\gamma-1)\left(I_2^2+I_3^2+I_4^2-2I_2I_5\right) = 0, \tag{2}$$

where γ is the specific heat ratio. Then the averaged pressure can be determined as

$$\overline{p} = \frac{I_2 \pm \sqrt{I_2^2+(\gamma^2-1)(I_2^2+I_3^2+I_4^2-2I_2I_5)}}{\gamma-1}, \tag{3}$$

where the positive and negative signs before the square root correspond to the subsonic and supersonic flows in axial direction, respectively. Then the other averaged flow variables can be calculated.

The non-reflective boundary conditions on both upstream and downstream sides can be determined according to the directions of characteristic waves and the averaged flow variables. Consider the subsonic case in the axial direction. For the normal flow on the interface, the total pressure, total temperature and flow angles in ghost cells are set by those from the upstream side, while the static pressure is provided by the downstream side. If the reversed flow happens on the interface, the static pressure from the upstream side and other variables from the downstream side are applied. For supersonic case, all flow variables in ghost cells are provided by the downstream or upstream sides depending on whether the reversed flow happens or not.

(2) Entropy-averaged (EA) model. It is well known that the fluid mixing inevitably produce additional entropy across the interface. The EA model is studied for the purpose of maintaining the interface entropy. The model is almost the same as MA model except replacing the axial momentum flux in eq. (1) by the entropy flux:

$$I_2 = \frac{1}{A_0}\int_A (\rho s v_x + p)\mathrm{d}A_x = \overline{\rho}\,\overline{s}\,\overline{v}_x + \overline{p}\,, \tag{4}$$

with the entropy defined as $s=p/\rho^{\gamma}$. Similarly, a nonlinear equation in density can be determined

$$a\overline{\rho}^{\,\gamma+2} + b\overline{\rho}^{\,\gamma+1} + I_1^2\overline{\rho}^{\,\gamma} + aI_1\overline{\rho}^{\,2} + I_1^3 = 0, \tag{5}$$

where $a = (I_3^2+I_4^2-2I_2I_5)/I_1^2$, $b = 2\gamma I_2/(\gamma-1)$. Since no analytical solution can be found for eq. (5), the Newton iteration method is employed to obtain the converged solution in ten iteration steps in the present study.

(3) Flux balanced model. The flux balance method [18] is sketched in Figure 1, where the flux differences between the upstream and downstream sides of the interface can be regarded as a group of error signals. After some algebraic work, the error signals can be described by the perturbations

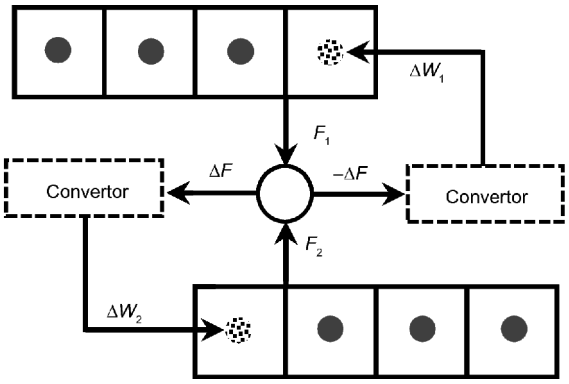

Figure 1 Sketch of flux balance method.

of characteristic variables, which are then transformed into the perturbations of conservation variables, while remaining the ones propagating into the interior of computation domain. Finally, the resultant perturbations of conservation variables are superimposed on the conservative ones at the ghost cells to accomplish the interface boundary conditions. The flux differences can be reduced to be zeros in principle when the computation converges. The mathematic descriptions of this method can be found in ref. [18], and the determinations of the interface boundary conditions can be found in ref. [28].

As with the simple mixing models, the flux on each side of the interface for the flux balanced MA (FBMA) and flux balanced EA (FBEA) methods can be calculated by eqs. (1) and (4), respectively.

2.2 Volume-weighted sliding mesh technique

The dual time-stepping method [29] is used in the study for unsteady flow computations. The convergence acceleration techniques used for steady flow computations are still valid. The unsteady terms in the governing equations are discretized by the second-order backward difference formula. By the blade scaling rule proposed by Rai [22], the periodic boundary conditions are still satisfied for each blade row. However, the interface boundary conditions in unsteady flow computations are implemented by the sliding mesh technique [30,31]. In the present paper, a volume-weighted interpolation method is introduced to exchange two-dimensional flow fields across the interface between adjacent blade rows.

Consider the interpolation of flow variables for the target cell ABCD-EFGH from the source cells connected with the quadrilateral ABCD on the interface, as shown in Figure 2. On the interface, the polygons produced by the intersection of quadrilateral ABCD and the source quadrilaterals are determined by the Sutherland-Hodgman algorithm [32]. The area ratio, λ, of the intersected polygon to the corresponding source quadrilateral can be obtained for each source cell. The volume weight to interpolate the flow variables in the target

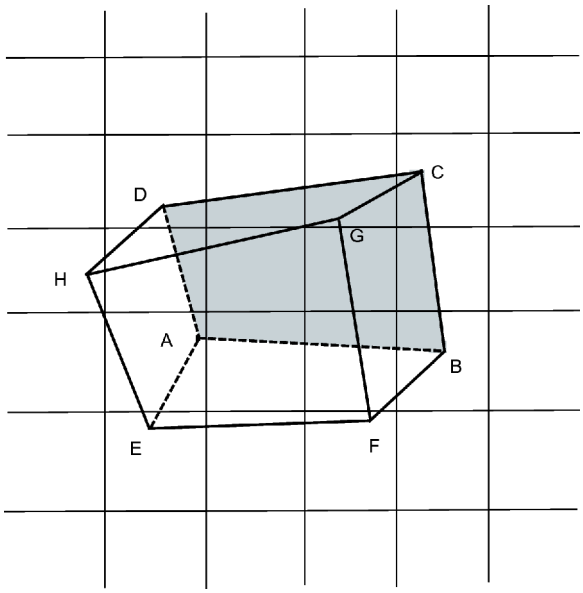

Figure 2 Sketch of cell connection on the interface.

cell ABCD-EFGH is given as

$$\varepsilon_i = \frac{\lambda_i V_i}{V_0},\ V_0 = \sum_{k=1}^{n} \lambda_k V_k,\ i = 1,\ 2,\ \ldots,\ n, \tag{6}$$

where n is the number of source cells and V_i the volume of the i-th source cell. The flow variables in the target cell *ABCD-EFGH* are then computed by

$$\mathbf{W} = \sum_{i=1}^{n} \mathbf{W}_i^S \varepsilon_i, \tag{7}$$

where $\mathbf{W}_i^S$ is the flow variables in the i-th source cell.

The flow variables in the target cell ABCD-EFGH are then assigned to the corresponding ghost cell to determine the interface boundary conditions. Since by the second-order finite volume method, the flow variables at the cell center can also be regarded as the volume-averaged ones, the present volume-weighted interpolation method can severely maintain the conservation of flow variables across the interface.

3 Flow solver validation

The validation of flow solver is carried out by comparing the numerical results of NASA Rotor 67 with the experiment. Rotor 67, which has been widely studied [33,34], is the first rotor of a transonic two-stage fan designed by NASA. The geometric and aerodynamic parameters can be found in refs. [35,36]. For the purpose of being used for the flow computations of multi-stages, the single passage of Rotor 67 is divided by two planes perpendicular to the axial direction into three parts, producing a quasi-1.5-stage transonic compressor, as shown in Figure 3. The positions of the two planes

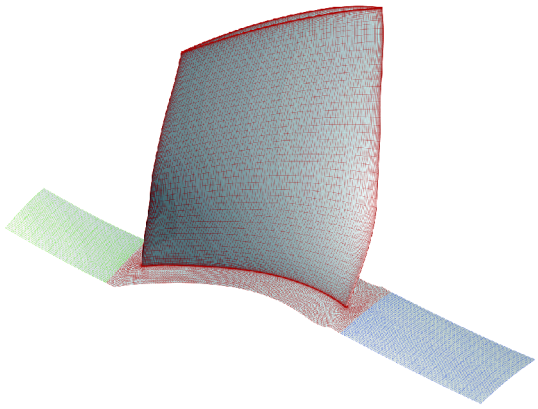

Figure 3 (Color online) Grid on the blade surface and hub of Rotor 67.

are chosen to make sure that the hub between the two planes is exactly the rotating portion in the experiment. The upstream and downstream parts are stationary, while the middle part rotates by the designed speed. The quasi-1.5-stage configuration, which is consistent with the experiment, is then used for the validations of flow solver and the studies of mixing models.

The total cell number of the multi-block grid is about 1.35 million with the dimensionless distance of the first point away from the wall $y^+<1$. The vertexes on the interfaces among neighboring blocks are strongly matched. In the study, a finer grid with doubled cells in the spanwise and pitchwise directions is used for flow computation. The aerodynamic parameters, such as total pressure ratio and total temperature ratio of the two grids deviate slightly from each other. Thus, the grid with 1.35 million cells is used in the study.

Figure 4 presents the operation characteristics of adiabatic efficiency and total pressure ratio, in which Exp, MP and TA stand for the results obtained from experiment, mixing model and time-averaged flow solutions, respectively. Since the aerodynamic parameters by the four mixing models are almost the same, only the results by MA model are shown herein. The mass flow rates of computation and experiment are normalized by the corresponding choked values. Generally, the computed total pressure ratio and adiabatic efficiency agree well with the experiment. The deviations are within the experiment tolerances. Compared with the time-averaged results, the computed ones by the mixing model are slightly larger. The reason can be found from the spanwise distributions of flow solutions, as presented following.

The spanwise distributions of circumferentially mass-averaged total pressure ratio and total temperature ratio are presented and compared with the experiment results at the operation condition near peak efficiency. The corresponding operating points of TA and MP computations are marked by 'Diamond' symbols in Figure 4. From Figure 5 it can be found that the computed aerodynamic parameters agree well

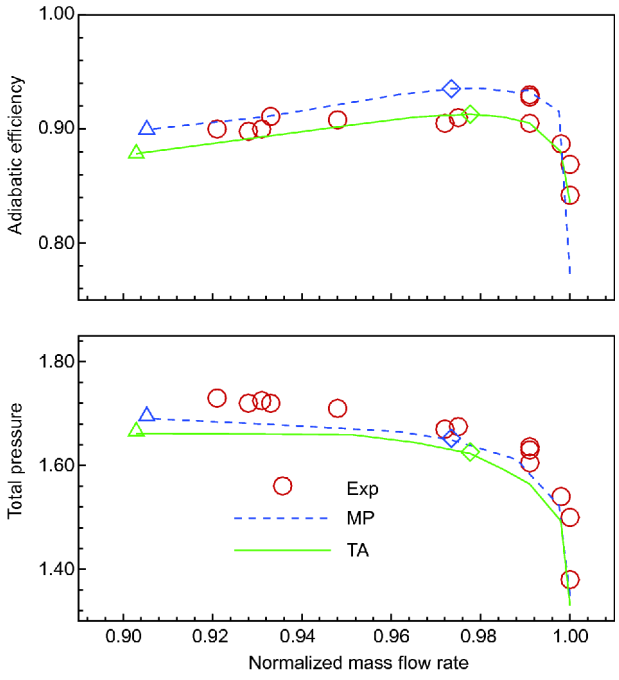

Figure 4 (Color online) Operation characteristics of Rotor 67.

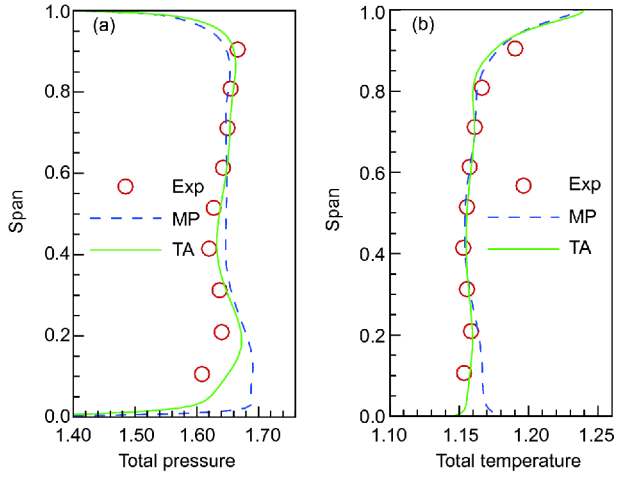

Figure 5 (Color online) Spanwise distributions of aerodynamic parameters at near peak efficiency point of Rotor 67. (a) Total pressure; (b) total temperature.

with the experiment on most spans except those near the hub. From hub to about 20% span, the time-averaged solutions perform better agreements with the experiment, while the mixing model results are evidently larger. On the spans near the casing, the time-averaged total pressure ratio is closer to the experiment. It is well known that the tip-leakage flow is unsteady, thus it can be resolved more accurately by the unsteady computation method.

Near the hub, the total pressure and total temperature by the mixing model evidently deviate from the time-averaged and experiment results due to an inherent shortage of mixing model. At the operation condition near peak efficiency, there exists a significant flow separation region near the hub. Figure 6 presents the contours of axial velocity at 3% span. Since the circumferential average is necessary in mixing model, the reversed flow will be escaped if the flow separation only takes up a small part in the pitchwise direction. In other words, the mixing model cannot capture the part-pitch flow separation on the interface, however, which can be captured by the unsteady computation. It can be found that there is no reversed flow on the second interface by the mixing model. Furthermore, compared with the unsteady computation, the separation point on the suction surface by the mixing model moves backward, and the wake region on the interface is significantly reduced. This is the reason why the overall aerodynamic parameters by the mixing model are larger than the time-averaged ones near the hub.

The spanwise distributions of total pressure ratio and total temperature ratio at the operation condition near stall are shown in Figure 7. The operating points of TA and MP computations are represented by 'Triangle' symbols in Figure 4. Near the hub, the time-averaged results agree better with the experiment than the mixing model solutions due to the still existing part-pitch flow separation at this operating point. Near the casing, both time-averaged and mixing model results slightly deviate from the experiment, which is attributed to the poor captures of tip leakage vortexes for both computational methods at the near stall operating point. The slightly lower total pressure ratio near the casing results in the smaller overall operation characteristics of computation methods in Figure 4.

4 Results and discussion

4.1 Case I: RWTH Aachen 1.5-stage turbine

A subsonic 1.5-stage axial turbine originally designed by RWTH Aachen University is firstly studied. The configuration of the turbine is Stator-Rotor-Stator. The untwisted low-

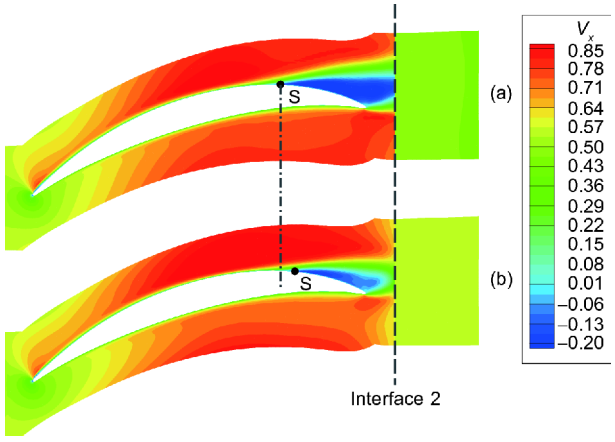

Figure 6 (Color online) Contours of axial velocity at 3% span of Rotor 67. (a) TA; (b) MP.

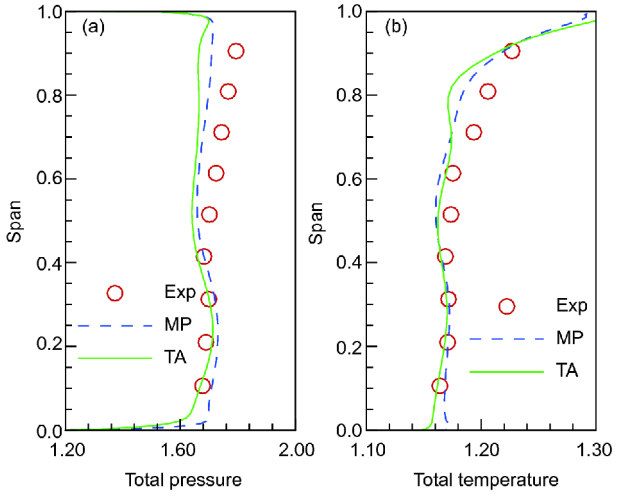

Figure 7 (Color online) Spanwise distributions of aerodynamic parameters at near stall point of Rotor 67. (a) Total pressure; (b) total temperature.

aspect-ratio blades are used for all blade rows. The details of geometric and aerodynamic parameters can be found in ref. [37]. To reduce the computing cost of unsteady flow computation, the blade numbers are scaled from 36:41:36 to 36:48:36 by the rule proposed by Rai [22]. In such situations, the unsteady computation can be performed for the modified multi-stage configuration with only three and four blade passages for the stators and rotor, respectively. The grid for steady computation is shown in Figure 8. The total cell number is about 1.32 million, while the total cell number for unsteady computation is about 4.53 million. The vertexes on the interfaces among neighboring blocks are strongly matched except those between adjacent blade rows. The spanwise distribution of total pressure, a constant total temperature and incidence angles at the inlet are given. For the unsteady flow computation, there are thirty physical time steps in one rotor passing period.

To verify the conservation of flow solutions across the interfaces, Tables 1 and 2 show the relative deviations of several flow variables across the first and second interfaces of the multi-stage turbine, respectively. $\dot{m}$, v_x, p, s, π and θ are mass flow rate, axial velocity, pressure, entropy, total pressure ratio and total temperature ratio, respectively. The relative deviation is defined as

$$\sigma_\phi = \frac{\phi_{\mathrm{dn}} - \phi_{\mathrm{up}}}{\max\left\{\left|\phi_{\mathrm{up}}\right|, \left|\phi_{\mathrm{dn}}\right|\right\}}, \tag{8}$$

where ϕ stands for the mass-averaged flow variables, the subscripts "*up*" and "*dn*" represent upstream and downstream of the interface. As shown in Tables 1 and 2, unsteady computation method performs much better on the conservation of most flow variables, indicating strong flow conservation across the interfaces by the present volume-weighted interpolation method. Compared with MA model,

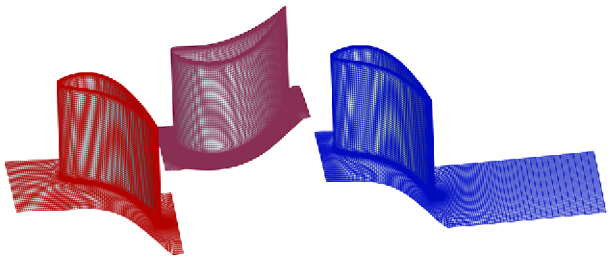

Figure 8 (Color online) Grid on the blade surface and hub of Aachen turbine.

Table 1 Relative deviations of flow variables across the 1st interface

Parameters	MA	EA	FBMA	FBEA	TA
$\dot{m}(\times10^{-4})$	1.58	0.76	0.49	0.48	−3.37
v_x $(\times10^{-4})$	−0.65	−1.01	−1.38	−1.38	−3.93
p $(\times10^{-4})$	−1.73	−1.46	−1.15	−1.14	−0.06
s $(\times10^{-4})$	1.10	−0.99	1.03	1.03	0.08
π $(\times10^{-4})$	−3.20	−3.02	−2.59	−2.58	−0.28
θ $(\times10^{-5})$	−0.60	6.00	2.10	2.00	−0.10

Table 2 Relative deviations of flow variables across the 2nd interface

Parameters	MA	EA	FBMA	FBEA	TA
$\dot{m}(\times10^{-5})$	4.20	−3.20	−4.60	−4.60	7.90
v_x $(\times10^{-4})$	−0.62	−1.06	−0.71	−0.71	−7.06
p $(\times10^{-4})$	−1.47	−1.22	−1.17	−1.15	−0.02
s $(\times10^{-4})$	0.70	0.59	0.49	0.49	0.28
π $(\times10^{-4})$	−2.36	−2.12	−2.03	−2.02	−0.54
θ $(\times10^{-5})$	−1.66	4.47	1.45	1.45	1.45

the entropy deviation of EA model is decreased, demonstrating the practicality of maintaining entropy flux in the mixing model. Generally, the flow variable deviations are very close between the FBMA and FBEA models. However, compared with the simple mixing models, the deviations are significantly reduced by the flux balanced models for most of the flow variables, such as the mass flow rate on the first interface, the entropy on the second interface, the pressure, total pressure ratio and total temperature ratio on both interfaces.

Besides upon the flow conservation across interfaces, computation methods also affect the overall aerodynamic parameters. Figures 9 and 10 present the spanwise distributions of total pressure ratio and total temperature ratio on the first and second interfaces, respectively. The spanwise distributions of total pressure ratio by the mixing models are almost the duplicates of each other; moreover, they are close enough with the time-averaged results. However, the spanwise distributions of total temperature ratio obtained from flux balanced models are quite different with those from the simple mixing models. Near the hub and casing on the first interface, the total temperature ratio of flux balanced models

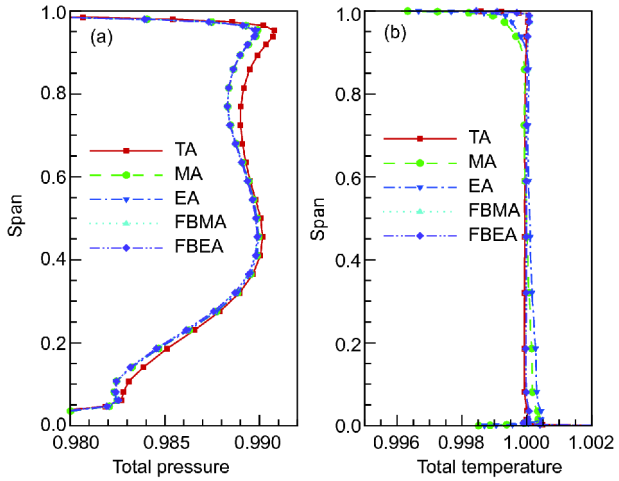

Figure 9 (Color online) Spanwise distributions of aerodynamic parameters on the 1st interface of Aachen turbine. (a) Total pressure ratio; (b) total temperature ratio.

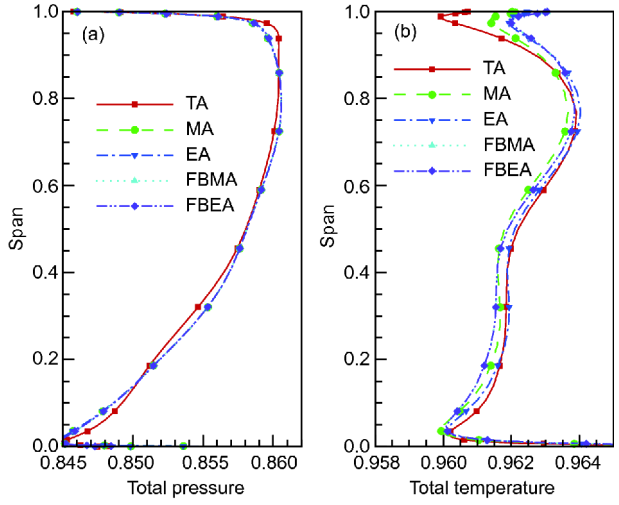

Figure 10 (Color online) Spanwise distributions of aerodynamic parameters on the 2nd interface of Aachen turbine. (a) Total pressure ratio; (b) total temperature ratio.

agree well with the time-averaged one, further demonstrating the effectiveness of flux balance technique in the mixing models. As a consequence of the deviations of total temperature ratio near the hub and casing on the first interface, the total temperature ratio significantly deviate from each other on the whole span between the simple and flux balanced mixing models.

4.2 Case II: Quasi-1.5-stage Rotor 67

To study the performance of flux balanced mixing models on simulating the complex flow, such as shock wave and reversed flow on the interface, the quasi-1.5-stage Rotor 67 with small geometric modification is then investigated. An artificial step of about 6% span is imposed on the casing contour ahead of the second interface to produce reversed flow on the interface. The designed and modified casing contours are shown in Figure 11. The grid with the same topology and cell number used for flow solver validation is generated.

Tables 3 and 4 list the relative deviations of flow variables across the first and second interfaces of the modified quasi-1.5-stage Rotor 67. v_θ is the circumferential velocity. On both interfaces, the unsteady computation has an absolute advantage on the flow conservation over all the mixing models. Compared with the simple mixing models, the relative deviations of most of flow variables are decreased by the flux balanced models. By the flux balanced models, the total temperature ratio across all the interfaces is almost strictly maintained, demonstrating the superior performance of flux balanced mixing models on flow conservation.

Compared with other flow variables, the relative deviation of tangential velocity across the first interface is extremely large, especially for MA and EA models. This is because the tangential velocity on the interface is quite small. The entropy by MA and EA models decreases across the first interface, violating the physical rule of entropy production. It is supposed to be induced by the large deviation of tangential velocity. The total pressure ratio by FBEA model slightly increases across the first interface, also violating the physical rule. It is supposed to be induced by the slightly increased entropy production across the interface. The entropy deviation of EA model is much larger than MA model on the second interface. This is because eq. (5) associated with EA model is a transcendental equation with multiple solutions and cannot be solved analytically. Affected by the part-pitch flow separation near the hub, the averaged density obtained from eq. (5) and thus the other flow variables may be non-physical solutions at several spans on the interface.

Figure 12 shows the spanwise distributions of total pres-

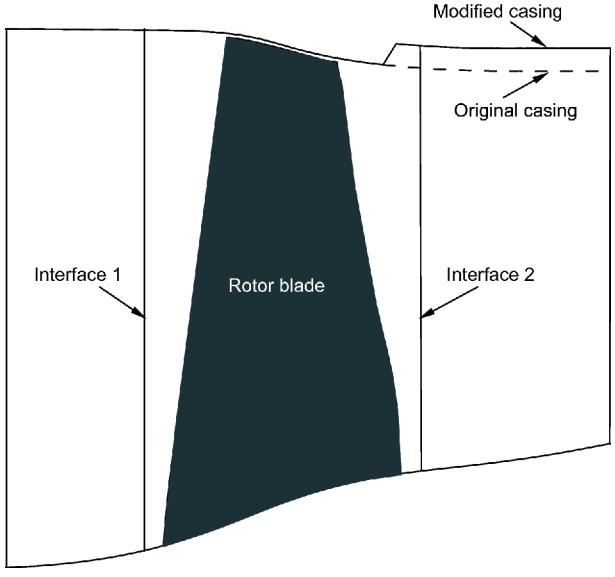

Figure 11 Sketch of casing treatment of Rotor 67.

Table 3 Relative deviations of flow variables across the 1st interface

Parameters	MA	EA	FBMA	FBEA	TA
$m(\times10^{-4})$	5.39	1.27	5.00	4.97	0.01
v_x $(\times10^{-3})$	1.42	0.38	1.20	0.22	0.01
v_θ $(\times10^{-0})$	−1.01	−1.01	−0.12	0.50	−0.04
p $(\times10^{-3})$	−1.66	−0.90	−0.89	−0.18	−0.01
s $(\times10^{-4})$	−6.80	−8.02	1.10	0.10	−0.03
π $(\times10^{-4})$	−8.58	−5.46	−3.62	0.43	0.01
θ $(\times10^{-4})$	−7.38	−7.36	−0.30	0.23	0.01

Table 4 Relative deviations of flow variables across the 2nd interface

Parameters	MA	EA	FBMA	FBEA	TA
$m(\times10^{-3})$	3.45	3.41	2.06	2.06	−0.07
v_x $(\times10^{-3})$	−4.65	−1.31	−4.24	−1.50	−0.19
v_θ $(\times10^{-3})$	1.48	1.53	1.25	−0.57	0.10
p $(\times10^{-3})$	0.65	2.36	0.39	−0.92	−0.01
s $(\times10^{-3})$	0.18	6.59	0.13	0.69	0.08
π $(\times10^{-3})$	−2.27	−1.11	−1.66	−1.88	−0.08
θ $(\times10^{-3})$	−0.43	4.57	0.15	−0.15	0.02

sure ratio and total temperature ratio on the first interface. The spanwise distributions of total pressure ratio by the mixing models perform ruleless variations, whereas the deviations from time-averaged ones are slight. The spanwise distributions of total temperature ratio by the simple mixing models are far away from the time-averaged distribution, whereas the ones obtained from flux balanced mixing models are almost the duplicates of time-averaged distribution.

The discrepancies of flow variables among the present methods on the middle and upper spans are associated with the shock wave. The shock wave originated from the leading edge of rotor blade injects onto the first interface, which can be illustrated by the contour of relative Mach number at 50% span in Figure 13. The position of shock wave on the interface can also be clearly displayed by the contour of static temperature in Figure 14. The shock wave injects onto the interface from 20% to 75% spans, where the spanwise distributions of flow variables by different computation methods are not consistent with each other as shown in Figure 12.

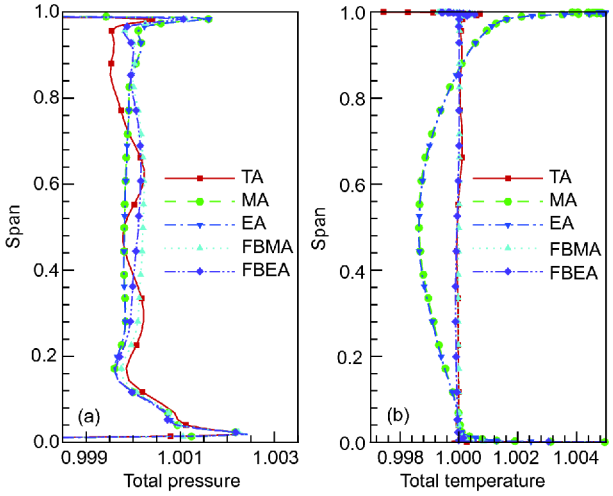

Figure 12 (Color online) Spanwise distributions of aerodynamic parameters on the 1st interface of modified Rotor 67. (a) Total pressure ratio; (b) total temperature ratio.

Although the positions of shock wave on the interface are almost the same for all the methods, the detailed shock wave patterns are slightly different as indicated by the zones with low static temperature in Figure 14. The shock wave patterns by MA and EA models are similar, and those by FBMA and FBEA models are also close, which are consistent with the spanwise distributions of total pressure ratio and total temperature ratio. However, none of shock wave patterns by the mixing models matches well with that of unsteady computation. The patterns of rarefaction waves after the shock waves perform the similar variations.

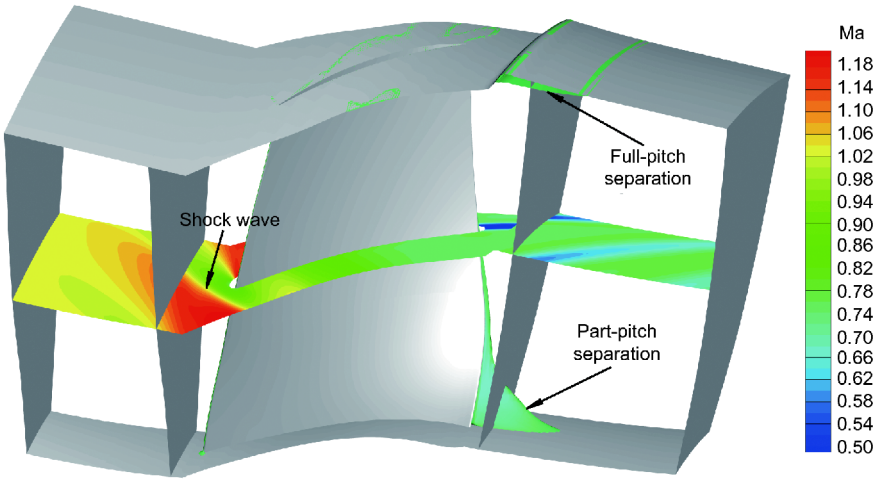

Figure 13 (Color online) Contour of relative Mach number and iso-surface of axial velocity of modified Rotor 67.

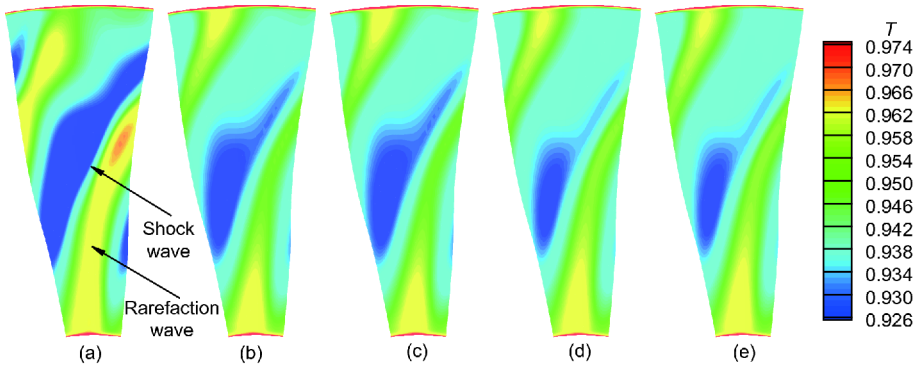

Figure 14 (Color online) Contours of temperature on the 1st interface of modified Rotor 67. (a) TA; (b) MA; (c) EA; (d) FBMA; (e) FBEA.

In Figure 13, the iso-surface of axial velocity with a small negative value is shown. It can be found that across the second interface, there is a full-pitch separation region near the casing caused by the artificial step and a part-pitch separation region near the hub caused by the flow separation on the blade suction surface. The spanwise distributions of flow variables on the second interface are shown in Figure 15, where the distributions on the top 4% span are enlarged in the upper right corners. Similar to those on the first interface, the spanwise distributions of flow variables obtained from mixing models are very close to each other, except the total temperature ratio. Moreover, the flow variables by different mixing models perform the same variations on most of the spans as the time-averaged ones, whereas significant discrepancies can be found near the casing and hub.

Near the hub, the spanwise variations of flow variables by the mixing models evidently differ from those by unsteady computation due to the inherent shortage of now available mixing models, as discussed in the section of flow solver validation. Although the part-pitch separation region exists below about 10% span as shown in Figure 13, the deviations between the mixing model-based flow variables and the time-averaged ones extend to a larger spanwise range because of the blockage effects near the hub, as shown in Figure 15.

By using the flux balanced mixing models, the spanwise distributions of aerodynamic parameters near the casing are improved. Compared with simple mixing models, the spanwise flow variations by the flux balanced models agree better with those by unsteady computation, which can be further validated by the pitchwise variations of axial velocity at 99% span on the second interface as shown in Figure 16. Besides, Figure 17 presents the contours of axial velocity on the blade-to-blade streamsurface at 99% span. By the flux balanced models, the deep blue contours near the second interface are closer to the unsteady contour, further demonstrating the ability of flux balanced models on distinguishing the reversed flow across the interface between adjacent blade rows, while the reversed flow is usually eliminated after flow averaging by using simple mixing models. In Figure 17, the axial locations of both separation and reattachment lines are almost the same for all the com-

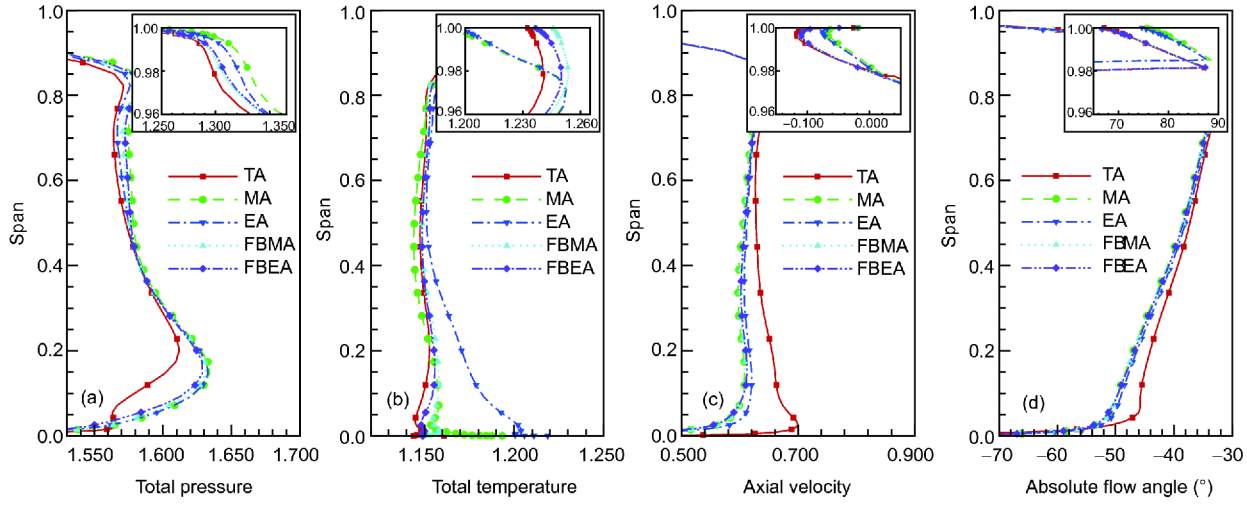

Figure 15 (Color online) Spanwise distributions of aerodynamic parameters on the 2nd interface of modified Rotor 67. (a) Total pressure ratio; (b) total temperature ratio; (c) axial velocity; (d) absolute flow angle.

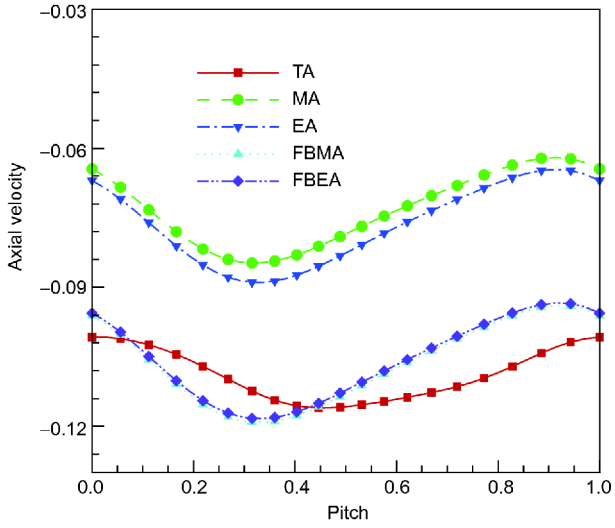

Figure 16 (Color online) Pitchwise variation of axial velocity at 99% span on the 2nd interface of modified Rotor 67.

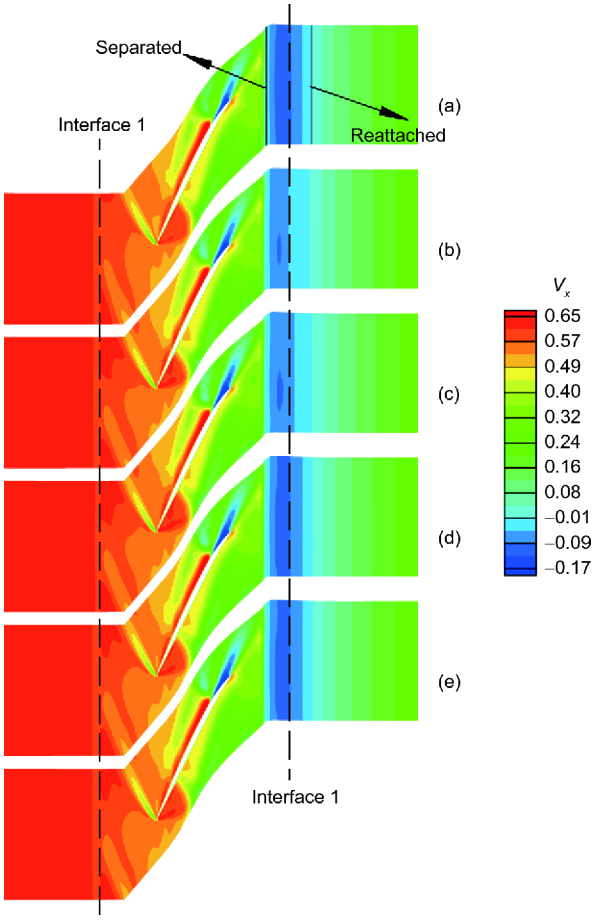

Figure 17 (Color online) Contours of axial velocity on the blade-to-blade streamsurface at 99% span of modified Rotor 67. (a) TA; (b) MA; (c) EA; (d) FBMA; (e) FBEA.

putation methods. However, it can be found from Figure 15 (d) that the flow separation regions in the spanwise direction by MA and EA models are slightly reduced, compared with the other methods.

Table 5 Aerodynamic parameters of modified Rotor 67

Parameters	TA	MA	EA	FBMA	FBEA
π	1.5591	1.5758	1.5708	1.5724	1.5741
θ	1.1531	1.1540	1.1634	1.1557	1.1553

The behaviours of the five different computation methods on the interfaces can inevitably affect the overall aerodynamic performance of the rotor. The total pressure ratio and total temperature ratio at the outlet are listed in Table 5. Generally, the total pressure ratio and total temperature ratio by the mixing models are slightly larger than those of time-averaged results, which is quite similar with the study on the designed Rotor 67 as presented in the section of flow solver validation. However, the aerodynamic parameters obtained from different flux balanced models are close enough to each other, while there exist evident deviations between different simple mixing models.

5 Conclusions

Mixing models and volume-weighted interpolation method are implemented and used for flow computations of multi-stage turbomachinery flow. A subsonic 1.5-stage axial turbine and a quasi-1.5-stage transonic compressor rotor by dividing the single passage into three blocks are investigated by using the simple and flux balanced mixing models, and the results are presented and compared with those obtained from unsteady computations in detail.

(1) The unsteady computation method performs excellently on flow conservation across the interface. Compared with the simple mixing models, stronger conservation can be achieved by using the flux balance technique for most of flow variables. Although the spanwise distributions of aerodynamic parameters on the interfaces cannot be close enough with those by unsteady computation, the ones obtained from flux balanced models match better compared with the simple models.

(2) Compared with the unsteady computation, the mixing models cannot accurately capture some detailed flow patterns on the interface, such as part-pitch flow separation. For some complex flows across the interface, such as injected shock wave, full-pitch flow separation, etc., the flux balanced mixing models perform comparatively better than the simple mixing models.

(3) Compared with the modified Rotor 67, the spanwise distributions of flow solutions, especially the total pressure ratio and axial velocity of Aachen axial turbine obtained from mixing models match better with the time-averaged ones. Generally, the shock wave injecting onto the first interface and the part-pitch separation on the second interface

induced by the corner flow separation lead to the difficulties on perfectly capturing the complex flow across the interface for all the mixing models. Without the detrimental effects of shock wave and flow separation, the computed results obtained from mixing models are more reliable.

This work was supported by the National Natural Science Foundation of China (Grant Nos. 51376009 & 51676003).

1 Wu C H. A general theory of three-dimensional flow in subsonic and supersonic turbomachines of axial-, radial-, and mixed-flow types. NASA TN 2604, 1952
2 Denton J D. The calculation of three dimensional viscous flow through multistage turbomachines. ASME, 1990. 90-GT-19
3 Adamczyk J J. Model equation for simulating flows in multistage turbomachinery. ASME, 1985. 85-GT-226
4 Adamczyk J J, Mulac R A, Celestina M L. A model for closing the inviscid form of the average-passage equation system. ASME, 1986. 86-GT-227
5 Erdos J I, Alzner E, McNally W. Numerical solution of periodic transonic flow through a fan stage. AIAA J, 1977, 15: 1559–1568
6 Giles M B. Calculation of unsteady wake/rotor interaction. J Propul Power, 1988, 4: 356–362
7 Hall E J. Aerodynamic modelling of multistage compressor flow fields Part 1: Analysis of rotor-stator-rotor aerodynamic interaction. Proc Inst Mech Eng Part G-J Aerosp Eng, 1998, 212: 77–89
8 Davis R L, Yao J. Prediction of compressor stage performance from choke through stall. J Propul Power, 2006, 22: 550–557
9 Gourdain N, Wlassow F, Ottavy X. Effect of tip clearance dimensions and control of unsteady flows in a multi-stage high-pressure compressor. J Turbomach, 2012, 134: 051005
10 Liu Y, Yu X, Liu B. Turbulence models assessment for large-scale tip vortices in an axial compressor rotor. J Propul Power, 2008, 24: 15–25
11 You D, Wang M, Moin P, et al. Effects of tip-gap size on the tip-leakage flow in a turbomachinery cascade. Phys Fluids, 2006, 18: 105102
12 You D, Wang M, Moin P, et al. Large-eddy simulation analysis of mechanisms for viscous losses in a turbomachinery tip-clearance flow. J Fluid Mech, 2007, 586: 177–204
13 Liu Y, Yan H, Lu L, et al. Investigation of vortical structures and turbulence characteristics in corner separation in a linear compressor cascade using DDES. J Fluids Eng, 2017, 139: 021107
14 Yan H, Liu Y, Li Q, et al. Turbulence characteristics in corner separation in a highly loaded linear compressor cascade. Aerosp Sci Tech, 2018, 75: 139–154
15 Saxer A P, Giles M B. Predictions of 3-D steady and unsteady inviscid transonic stator/rotor interaction with inlet radial temperature nonuniformity. ASME, 1993. 93-GT-10
16 Chima R V. Calculation of multistage turbomachinery using steady characteristic boundary conditions. AIAA, 1998. 98-0968
17 Hanimann L, Mangani L, Casartelli E, et al. Development of a novel mixing plane interface using a fully implicit averaging for stage analysis. J Turbomach, 2014, 136: 081010
18 Holmes D G. Mixing planes revisited: A steady mixing plane approach designed to combine high levels of conservation and robustness. ASME, 2008. GT2008-51296
19 Wang D X. An improved mixing-plane method for analyzing steady flow through multiple-blade-row turbomachines. J Turbomach, 2014, 136: 081003
20 Ning F. MAP: CFD package for turbomachinery flow simulation and aerodynamic design optimization. ASME, 2014. GT2014-26515
21 Du P, Ning F. Validation of a novel mixing-plane method for multi-stage turbomachinery steady flow analysis. Chin J Aeronaut, 2016, 29: 1563–1574
22 Rai M M. Navier-Stokes simulations of rotor/stator interaction using patched and overlaid grids. J Propul Power, 1987, 3: 387–396
23 He L, Ning W. Efficient approach for analysis of unsteady viscous flows in turbomachines. AIAA J, 1998, 36: 2005–2012
24 Hall K C, Clark W S, Thomas J P. Computation of unsteady nonlinear flows in cascades using a harmonic balance technique. AIAA J, 2002, 40: 879–886
25 Spalart P A, Allmaras S R. A one-equation turbulence model for aerodynamic flows. AIAA, 1992. 92-0439
26 Jameson A, Schmidt W, Turkel E. Numerical solution of the Euler equations by finite volume methods using Runge-Kutta time stepping schemes. AIAA, 1981. 81-1259
27 Yoon S, Jameson A. Lower-upper symmetric-Gauss-Seidel method for the Euler and Navier-Stokes equations. AIAA J, 1988, 26: 1025–1026
28 Vasanthakumar P. Three dimensional frequency-domain solution method for unsteady turbomachinery flows. Doctoral Dissertation. Durham: Durham University, 2003
29 Jameson A. Time dependent calculations using multigrid, with applications to unsteady flows past airfoils and wings. AIAA, 1991. 91-1596
30 Rai M M. A conservative treatment of zonal boundaries for Euler equation calculations. J Comput Phys, 1986, 62: 472–503
31 Rai M M. A relaxation approach to patched-grid calculations with the Euler equations. J Comput Phys, 1986, 66: 99–131
32 Sutherland I E, Hodgman G W. Reentrant polygon clipping. Commun ACM, 1974, 17: 32–42
33 Luo J, Zhou C, Liu F. Multipoint design optimization of a transonic compressor blade by using an adjoint method. J Turbomach, 2014, 136: 051005
34 Tang X, Luo J, Liu F. Aerodynamic shape optimization of a transonic fan by an adjoint-response surface method. Aerosp Sci Tech, 2017, 68: 26–36
35 Urasek D C, Gorrell W T, Cunnan W S. Performance of two-stage fan having low-aspect-ratio first-stage rotor blading. NASA Technical Report 1493, 1979
36 Strazisar A J, Wood J R, Hathaway M D, et al. Laser anemometer measurements in a transonic axial-flow fan rotor. NASA Technical Report 2879, 1989
37 Stephan B, Gallus H E, Niehuis R. Experimental investigations of tip clearance flow and its influence on secondary flows in a 1-1/2 stage axial turbine. ASME, 2000. 2000-GT-613